

Check for updates

## **Bimetallic Nanocluster-Based Light-Emitting Diodes With** High External Quantum Efficiency and Saturated Red **Fmission**

Jose V. Rival, Savita Chand, Arijit Jana, Nonappa, Vasudevanpillai Biju, Thalappil Pradeep, Pachaiyappan Rajamalli,\* and Edakkattuparambil Sidharth Shibu\*

Dedicated to Professor Vijayamohanan K Pillai on the occasion of his 65th Birthday

Self-emissive atomically precise metal nanoclusters (NCs) are emerging as promising emissive layer material for next-generation light-emitting diodes (LEDs), thanks to their solid-state luminescence, well-defined structures, photo/thermal stability, low toxicity, and unique excited-state properties. However, achieving high external quantum efficiency (EQE) in solid-state NCs remains a formidable challenge. In this study, a highly stable bimetallic gold-copper NC forming [Au<sub>2</sub>Cu<sub>6</sub>(Sadm)<sub>6</sub>(DPPEO)<sub>2</sub>] stabilized with 1-adamantanethiol (HSadm) and 1,2-bis(diphenylphosphino)ethane (DPPE) as the primary and secondary ligands, respectively is reported. Single-crystal X-ray diffraction and spectroscopic analyses suggest that the as-synthesized NC contains one phosphine bound to gold and the second phosphine has oxidized to phosphine oxide (P=O). The presence of such P=O moieties in the NC facilitated C-H···O interactions along with C-H··· $\pi$  and H···H interactions between ligands, promoting rapid crystallization. Due to the exceptional photo/thermal stability and enhanced solid-state photoluminescence quantum yield (PLQY), [Au<sub>2</sub>Cu<sub>6</sub>(Sadm)<sub>6</sub>(DPPEO)<sub>2</sub>] NC is utilized to fabricate the NC-based LED (NC-LED) via the solution-processed technique, without using any additional host materials. The fabricated NC-LED shows a maximum brightness of 1246 cd m<sup>-2</sup> and an EQE of 12.60% with a pure red emission ≈668 nm. This EQE value coupled with saturated pure red emission is the best among solution-processed and non-doped NC-LEDs, suggesting the enormous potential of the NCs for electro-optical devices.

#### 1. Introduction

Self-emissive light-emitting diodes (LEDs) have received significant attention in recent years due to their reduced energy consumption, environmental compatibility, and cost-effectiveness compared to conventional cathode-ray tube (CRT) and liquid crystal display (LCD) technologies.[1,2] In the past few decades, organic (OLED), polymer (PLED), quantum dot (QLED), and emerging perovskite-based LEDs (PeLED) have been successfully developed using emissive organic molecules, polymers, inorganic nanocrystals, and organic/inorganic hybrid materials, respectively.[3-8] Though all these emissive materials offer unique advantages, they face challenges such as laborious, high-temperature, and multiple synthesis steps, minimal structural selection, resource sustainability, toxicity, the requirement of passivating agents, and instability under light, heat, and moisture.[9-11] In this context, atomically precise nanoclusters (NCs) have emerged as promising materials for simple and low-cost solution processing devices. This is attributed to their easy synthetic routes,

J. V. Rival, E. S. Shibu Smart Materials Lab (SML) Department of Nanoscience and Technology (DNST) University of Calicut (UoC) Thenhipalam, Kerala 673635, India E-mail: shibu@uoc.ac.in

S. Chand, P. Rajamalli Materials Research Centre Indian Institute of Science Bangalore 560012, India E-mail: rajamalli@iisc.ac.in

The ORCID identification number(s) for the author(s) of this article

can be found under https://doi.org/10.1002/adma.202507893

Indian Institute of Technology Madras Chennai 600036, India Nonappa Faculty of Engineering and Natural Sciences **Tampere University** P.O. Box 541, Tampere FI-33101, Finland V. Biju Research Institute for Electronic Science Hokkaido University N20 W10, Sapporo, Hokkaido 001-0020, Japan

DST Unit of Nanoscience (DST UNS) and Thematic Unit of Excellence

A. Jana, T. Pradeep

Department of Chemistry

DOI: 10.1002/adma.202507893

15214055, 2025, 35, Dowloaded from https://abranced.online.bitabry.wiely.com/oi/010.1002adma.2025/993 by Edakatunparambil Sidharth Shibu - University Of Calicu, Wiley Online Library on [07/99/2025], See the Terms and Conditions (https://oininelibrary.wiely.com/etms-and-conditions) on Wiley Online Library for rules of use; OA articles are governed by the apaptic between the common in Library on [07/99/2025]. See the Terms and Conditions (https://oininelibrary.wiely.com/etms-and-conditions) on Wiley Online Library for rules of use; OA articles are governed by the apaptic between [07/99/2025]. See the Terms and Conditions (https://oininelibrary.wiely.com/etms-and-conditions) on Wiley Online Library for rules of use; OA articles are governed by the apaptic between [07/99/2025]. See the Terms and Conditions (https://oininelibrary.wiely.com/etms-and-conditions) on Wiley Online Library for rules of use; OA articles are governed by the apaptic between [07/99/2025]. See the Terms and Conditions (https://oininelibrary.wiely.com/etms-and-conditions) on Wiley Online Library for rules of use; OA articles are governed by the apaptic between [07/99/2025]. See the Terms and Conditions (https://oininelibrary.wiely.com/etms-and-conditions) on Wiley Online Library for rules of use; OA articles are governed by the apaptic between [07/99/2025]. See the Terms and Conditions (https://oininelibrary.wiely.com/etms-and-conditions) on the apaptic between [07/99/2025]. See the Terms and Conditions (https://oininelibrary.wiely.com/etms-and-conditions) on the apaptic between [07/99/2025]. See the Terms and Conditions (https://oininelibrary.wiely.com/etms-and-conditions) on the apaptic between [07/99/2025]. See the Terms and Conditions (https://oininelibrary.wiely.com/etms-and-conditions) on the apaptic between [07/99/2025].

low toxicity, well-defined crystal structure, unique excited state characteristics, photo/thermal stability, environmental compatibility, and solid-state photoluminescence (PL).[12-23] Although the external quantum efficiency (EQE) of NC-based LED (NC-LED) was initially below 0.1%,[24] a significant improvement has been made by combining them with various host materials.[18,25-31] However, the low PL quantum yield (PLQY), poor device compatibility due to the bulky ligands, and the need to incorporate additional host materials to achieve adequate conductivity continue limiting their applications in NC-LEDs.[32,33] Recent developments in metal core engineering, ligand engineering, selfassembly techniques, and advanced synthetic procedures significantly helped to overcome such issues.[34-44] The solid-state emitting NCs with improved PL properties have been recently developed using a combination of rigid ligands and multiple metal precursors.[45-47] Metal core/ligand engineering has reduced the PLQY gap between NCs and traditional luminescent materials by precisely controlling the core size, composition, and crystal structure. [48-57] However, developing an ideal blend of solid-state emitting NCs holding improved EQE is still in its infancy. To address this challenge, herein, we have designed and synthesized, highly stable and solid-state emitting gold-copper bimetallic NCs ([Au<sub>2</sub>Cu<sub>6</sub>(Sadm)<sub>6</sub>(DPPEO)<sub>2</sub>]) using 1-adamantanethiol (HSadm) and 1,2-bis(diphenylphosphino)ethane (DPPE) as the primary and secondary ligands, respectively. [Au<sub>2</sub>Cu<sub>6</sub>(Sadm)<sub>6</sub>(DPPEO)<sub>2</sub>] NCs were readily crystallized compared to previously reported analog ([Au<sub>2</sub>Cu<sub>6</sub>(Sadm)<sub>6</sub>(TPP)<sub>2</sub>]; TPP: triphenylphosphine) NC.[58,59] The electrospray ionization mass spectrometry (ESI-MS) and single crystal X-ray diffraction (SC-XRD) data suggest that only one phosphine is bound to the gold. The second phosphine ligand is oxidized to phosphine oxide ([Au<sub>2</sub>Cu<sub>6</sub>(Sadm)<sub>6</sub>(DPPEO)<sub>2</sub>]), as confirmed by various spectroscopic analyses. Such electron-withdrawing P=O moieties are known to offer enhanced electron transport apart from their ability to form uniform thin films and resist chemical and oxidative stress.[60-62] Moreover, due to the exceptional thermal and photostability of solid-state emitting [Au<sub>2</sub>Cu<sub>6</sub>(Sadm)<sub>6</sub>(DPPEO)<sub>2</sub>] NCs, we fabricated LEDs using this NC as an emitter. The solution-processed and non-doped NC-LEDs showed a maximum luminance of 1246 cd m<sup>-2</sup> and EQE of 12.60%. The electroluminescence (EL) maximum of the device was ≈668 nm with a turn-on voltage of 3V. The International Commission on Illumination (CIE) chromaticity coordinates (0.70, 0.30) at the edge of the chromaticity diagram represent an extremely saturated pure red emission. These NCs with enhanced PL, better thermal/photostability, and high device performance are expected to offer new directions in designing and fabricating efficient and non-toxic NC-LEDs for future sustainable technology.

## 2. Results and Discussion

**Figure 1a** shows the chemical structure of ligands (HSadm and DPPE) and the photographs of the reaction mixture during various steps of NC synthesis. The synthesis of bimetallic gold-copper  $[Au_2Cu_6(Sadm)_6(DPPEO)_2]$  NC was performed using a modified one-pot chemical reduction method reported previously for the synthesis of  $[Au_2Cu_6(Sadm)_6(TPP)_2]$  NCs (see Experimental Section for the details). [58] The introduc-

tion of DPPE ligands instead of TPP helped to reduce the amount of gold precursor and improved the yield and synthetic purity of NC. Similar to [Au<sub>2</sub>Cu<sub>4</sub>(Sadm)<sub>4</sub>(TPP)<sub>2</sub>] NC. the as-synthesized [Au<sub>2</sub>Cu<sub>6</sub>(Sadm)<sub>6</sub>(DPPEO)<sub>2</sub>] NCs in a solution and powder show purple under visible light and exhibit strong red emission under UV light (Figure 1b). The absorption spectra of [Au<sub>2</sub>Cu<sub>6</sub>(Sadm)<sub>6</sub>(DPPEO)<sub>2</sub>] (Figure 1d; d<sub>1</sub>(i)) and  $[Au_2Cu_6(Sadm)_6(TPP)_2]$  (Figure 1d;  $d_2(i)$ ) NCs in toluene and dichloromethane (DCM), respectively, exhibit multiple absorption peaks at 325, 425, 515, and 592 nm (Figure 1d), with no observable shift in these regions.<sup>[63]</sup> The PL spectrum of [Au<sub>2</sub>Cu<sub>6</sub>(Sadm)<sub>6</sub>(DPPEO)<sub>2</sub>] NCs (Figure 1d<sub>1</sub>; iii) displays two distinct emission maxima ≈675 and 798 nm when excited at 515 nm. In contrast, the PL spectrum of [Au<sub>2</sub>Cu<sub>6</sub>(Sadm)<sub>6</sub>(TPP)<sub>2</sub>] NCs (Figure  $1d_2$ ; iii) shows emission maxima  $\approx$ 675 and 806 nm at the same excitation wavelength. Notably, the excitation spectra corresponding to emission  $\approx 675$  nm (ii) of both NCs (d<sub>1</sub> and d<sub>2</sub>) closely resemble their respective absorption spectra (i), suggesting that the optical transitions are directly linked to the same electronic states, confirming a well-defined absorption-emission relationship in both systems. Similarly, the excitation spectra corresponding to the emissions ≈798 and 806 nm in the respective NCs also match with their absorbance spectra (Figure \$1, Supporting Information). The ESI-MS spectra showed molecular ion peaks  $\approx$ m/z 2607.78 (e<sub>1</sub>) and m/z 2303.52 (e<sub>2</sub>) correspond to the parent molecular ions of [Au<sub>2</sub>Cu<sub>6</sub>(Sadm)<sub>6</sub>(DPPEO)<sub>2</sub>] and [Au<sub>2</sub>Cu<sub>6</sub>(Sadm)<sub>6</sub>(TPP)<sub>2</sub>] NCs (Figure 1e), in which both the experimental and simulated m/z values are in good agreement (inset in Figure 1e). The oxidation of one unbound phosphine group from each DPPE ligand, leading to the formation of a P=O bond, is evident from the observed m/z value. This result indicates that, during the synthesis of the NCs, only one phosphine group from each DPPE molecule directly coordinates with the Au center, while the second phosphine undergoes oxidation to form a phosphine oxide (P=O).

To further confirm the presence of bound ligands in the purified [Au<sub>2</sub>Cu<sub>6</sub>(Sadm)<sub>6</sub>(DPPEO)<sub>2</sub>] NC, <sup>1</sup>H, and <sup>31</sup>P nuclear magnetic resonance (NMR) spectra were measured in CDCl<sub>2</sub> (Figures S2 and S3, Supporting Information). The <sup>1</sup>H chemical shifts at  $\delta = 7.85 - 7.79, 7.69 - 7.63, 7.46 - 7.40, 7.38 - 7.32, 7.30 - 7.27, 2.95,$ and 2.69 ppm represent combined aromatic (-Ph) and aliphatic (-CH<sub>2</sub>-CH<sub>2</sub>-) chains of DPPEO ligand, and the peaks at 1.95–1.87 and 1.62-1.44 ppm represent adamantane moieties. The splitting and downfield shift of the broad aromatic peak  $\approx \delta = 7.28$  ppm, and the aliphatic triplet ≈2.06 ppm, in the <sup>1</sup>H NMR spectrum of the DPPE ligand confirm the conversion of unbound phosphine to the P=O bond. At the same time, the presence of two types of phosphines (bound and P=O) was observed in the <sup>31</sup>P NMR spectrum of NCs (Figure S3, Supporting Information). DPPE showed only a single peak at -12.5 ppm, while an apparent splitting and downfield shift (33.7 and 60.4 ppm) were observed in the case of NCs owing to the presence of anchored phosphine on the NC surface and free-standing phosphine bound to an electronegative oxygen atom. NCs were further characterized using transmission electron microscopy (TEM) imaging. Although the TEM images (Figure 1c) showed a nearly uniform size distribution, it is important to note that due to electron beam-induced fusion of [Au<sub>2</sub>Cu<sub>6</sub>(Sadm)<sub>6</sub>(DPPEO)<sub>2</sub>] NCs, a few bigger particles were also observed during imaging. The X-ray photoelectron spectroscopy

15214095, 2025, 35, Downloaded from https://advanced.onlinelibrary.wiley

.com/doi/10.1002/adma.202507893 by Edakkattuparambil Sidharth Shibu - University Of Calicut , Wiley Online Library on [07/09/2025]. See the Terms

onditions) on Wiley Online Library for rules of use; OA articles are governed by the applicable Creative Commons License

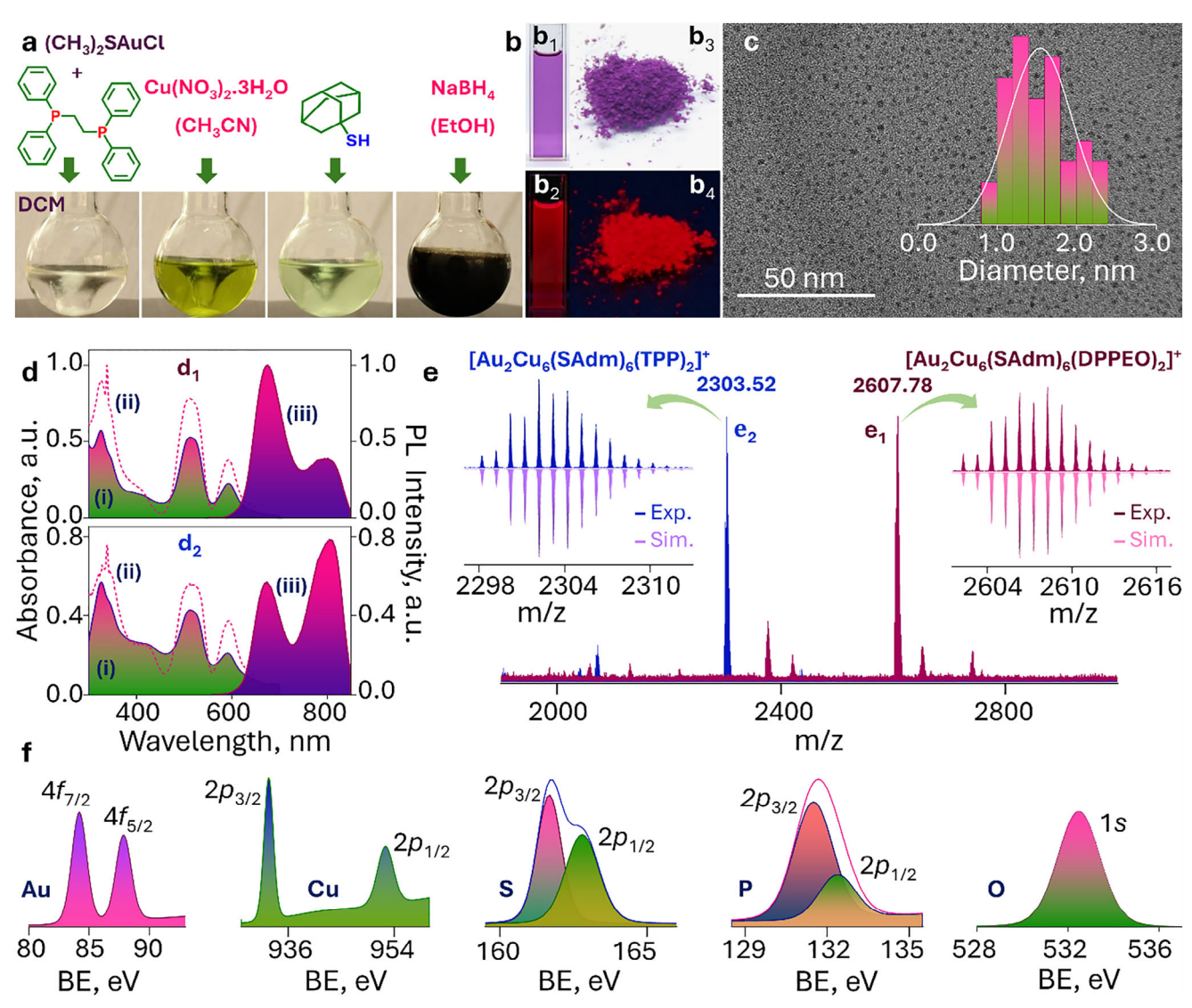


Figure 1. a) The photographs of reaction mixture showing different stages of  $[Au_2Cu_6(Sadm)_6(DPPEO)_2]$  NC synthesis and the chemical structure of DPPE and HSadm ligands. b) Photographs of  $[Au_2Cu_6(Sadm)_6(DPPEO)_2]$  NC solution  $(b_1$  and  $b_2)$ , and powder  $(b_3$  and  $b_4)$  captured under visible  $(b_1$  and  $b_3)$  and UV  $(b_2$  and  $b_4)$  lights. c) TEM micrograph of NCs with size distribution in the inset. d) UV/Vis absorption (i), excitation (ii), and PL (iii) spectra of  $[Au_2Cu_6(Sadm)_6(DPPEO)_2]$  NCs in toluene  $(d_1)$  and  $[Au_2Cu_6(Sadm)_6(TPP)_2]$  NCs in DCM  $(d_2)$ . e) The ESI-MS of  $(e_1)$   $[Au_2Cu_6(Sadm)_6(DPPEO)_2]$  and  $(e_2)$   $[Au_2Cu_6(Sadm)_6(TPP)_2]$  NCs. The inset shows the isotopic distribution of the experimental and simulated spectra. f) XPS spectral regions of  $[Au_2Cu_6(Sadm)_6(DPPEO)_2]$  NCs, showing gold, copper, sulfur, phosphorus, and oxygen fingerprints.

(XPS) analysis revealed binding energy (BE) values of Au 4f and Cu 2p levels closely match with the previous report, <sup>[58]</sup> which showed the presence of zero valence state gold (84.2 and 87.9 eV for Au  $4f_{7/2}$  and Au  $4f_{5/2}$ , respectively) and +1 valence state copper (952.5 and 932.7 eV for Cu  $2p_{3/2}$  and Cu  $2p_{1/2}$ , respectively) (Figure 1f). The S 2p binding energy values (161.7 and 162.8 eV for S  $2p_{3/2}$  and S  $2p_{1/2}$ , respectively) were consistent with thiolate binding, providing insights into the role of sulfur in the structure of NC. Further analysis unveiled P  $2p_{3/2}$  and  $2p_{1/2}$  peaks at 131.5 and 132.4 eV, respectively, along with an O 1s peak at 531.5 eV, confirming the presence of oxidized and bound DPPE within the NC. Though the two P atoms in each DPPE are different, it was difficult to differentiate them in XPS as the binding energies of Au-bound phosphine and P=O bonds are nearly identical.

Crystallization offers high-purity and quality single crystals for SC-XRD analysis to gain insight into molecular structure, packing, and inter-NC interactions. The solvent evaporation from the supersaturated toluene solution of [Au<sub>2</sub>Cu<sub>6</sub>(Sadm)<sub>6</sub>(DPPEO)<sub>2</sub>] NC resulted in rod-like single crystals, which displayed red emission upon UV illumination (**Figure 2a**–c). The SC-XRD studies showed that the NCs crystallized in a triclinic crystal system with a *P-1* space group (cif file is provided). The core structure was found to be similar to that of earlier reported [Au<sub>2</sub>Cu<sub>6</sub>(Sadm)<sub>6</sub>(TPP)<sub>2</sub>] NC (Figure 2d–f).<sup>[58]</sup> Figure 2d shows that the NC's central kernel consists of a benzenoid-like hexagonal planar copper (Cu<sub>6</sub>) framework with an average intermetallic Cu—Cu distance of 2.67 Å. Two isolated gold atoms were capped on the top and bottom of the Cu<sub>6</sub>, giving rise to a

15214095, 2025, 35, Dowlooded from https://a/vanced.online/barry.wiley.com/doi/10.1002adma.202578993 by Edakataparambil Sidharth Shibu - University Of Calicut. Wiley Online Library on [07/09/2025]. See the Terms and Conditions (https://oininelibrary.wiley.com/terms-and-conditions) on Wiley Online Library for rules of use, OA articles are governed by the applicable Decarity Comments.

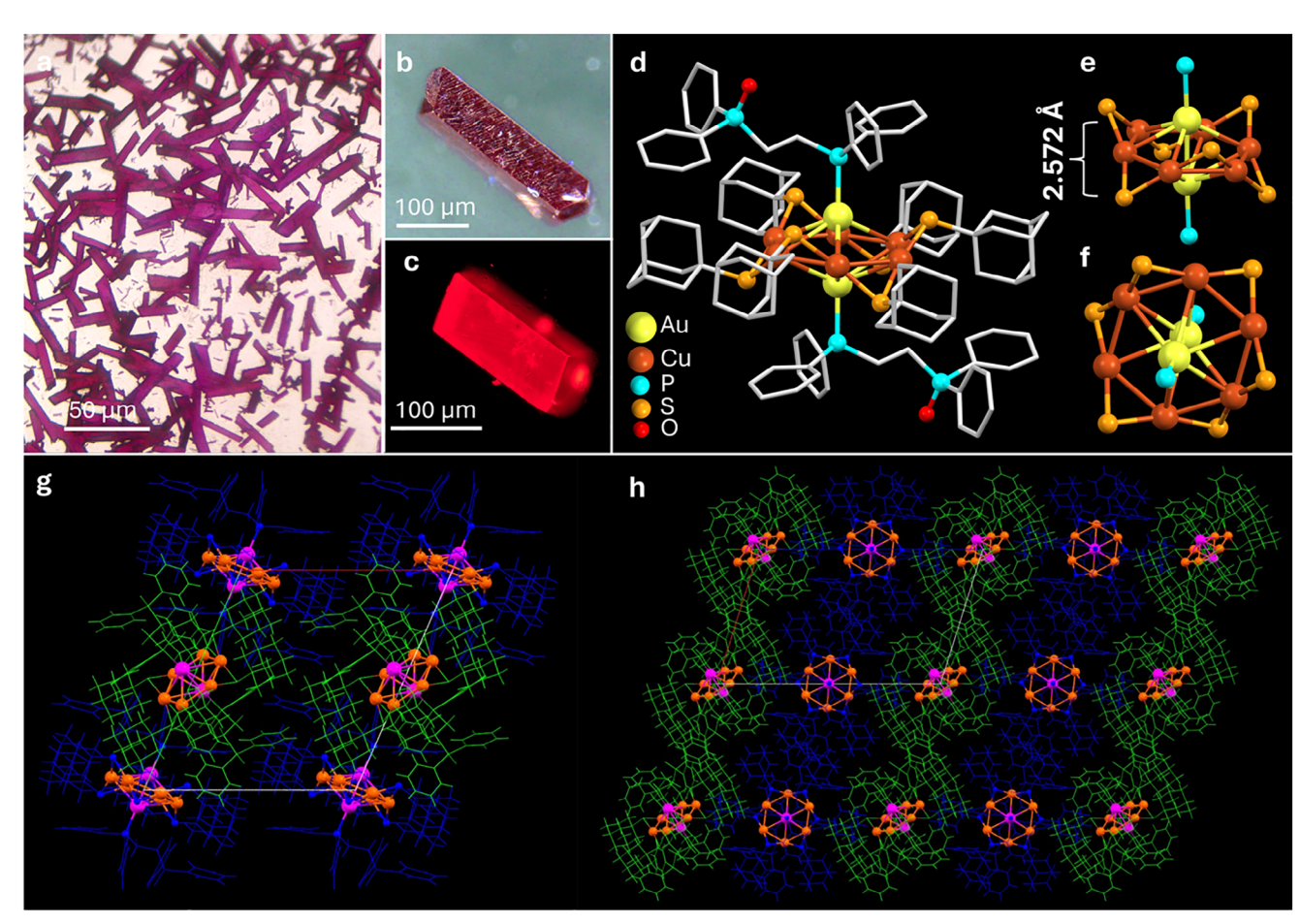


Figure 2. a) Large area optical microscopic image shows rod-like  $[Au_2Cu_6(Sadm)_6(DPPEO)_2]$  crystals. The optical image under white light and fluorescence image under 435 nm excitation of a single-crystal are shown in Figures b and c, respectively. d) Crystal structure of  $[Au_2Cu_6(Sadm)_6(DPPEO)_2]$  NC (hydrogen atoms omitted for clarity). e,f) The core of  $[Au_2Cu_6(Sadm)_6(DPPEO)_2]$  NC, viewed from two perpendicular projections. g) Unit cell molecular packing of NCs. h) The extended supramolecular packing shows a slanted layer-like lamellar arrangement of  $[Au_2Cu_6(Sadm)_6(DPPEO)_2]$  NCs.

hexagonal-bipyramidal geometry resembling the unidentified flying object (UFO)-like shape. The Cu-Au distance ranges from 2.8 to 3.0 Å, and the distance between two Au atoms is 2.572 Å. Six adamantane-thiolate is bonded with the hexagonal Cu<sub>6</sub>, where each -Sadm is tied with the Cu-Cu edge of the hexagon through 'V-shaped' Cu-S-Cu motifs (Figure 2e). The average Cu-S distance is 2.1 Å and the Cu-S-Cu angle ranges from 73.87° to 76.03°. The overall arrangement of the six S atoms can be visualized as a chair-shaped S<sub>6</sub> unit, where alternative S atoms are placed up and down the hexagonal Cu<sub>6</sub> unit. 3D adamantane units are placed in the central body of the NC in a planar fashion, and they sterically protect the NCs. Furthermore, two secondary DPPEO ligands were independently anchored on each gold atom (Figure 2d), where one phosphine was connected with the Au atom having an Au-P bond distance of 2.34 Å, and another phosphine underwent oxidation to form a robust P=O bond. This P=O bond is recognized as an effective hydrogen bond acceptor and often forms strong hydrogen bonds, typically with polar donor groups such as hydroxyls or amines.[62] However, the absence of such strong hydrogen bonding donors in [Au<sub>2</sub>Cu<sub>6</sub>(Sadm)<sub>6</sub>(DPPEO)<sub>2</sub>] NCs resulted in the C—H···O interactions between phosphine oxide and adamantane

hydrogens. This facilitated the formation of NC dimers, which further extended into a zig-zag tape arrangement (Figure S4, Supporting Information). In addition to this, C—H… $\pi$  and H…H interactions between the ligands also contributed to molecular packing, stabilizing crystal growth. The extended supramolecular packing reveals a slanted layer-like lamellar arrangement of NCs (Figure 2g,h). In comparison to the previously reported [Au<sub>2</sub>Cu<sub>6</sub>(Sadm)<sub>6</sub>(TPP)<sub>2</sub>] NC, [<sup>64</sup>] the presence of phosphine oxide in [Au<sub>2</sub>Cu<sub>6</sub>(Sadm)<sub>6</sub>(DPPEO)<sub>2</sub>] NCs induces a distinct orientation in alternating layers, driven by C—H…O interactions. The distance between two adjacent layers is 16.32 and 9.18 Å along a and b crystallographic directions, respectively.

To understand the emission mechanism of NC, we evaluated the optical absorption and PL behavior of  $[Au_2Cu_6(Sadm)_6(DPPEO)_2]$  NC solution (toluene) under nitrogen and oxygen atmospheres. The PL intensity of the NC solution (both 675 nm and 798 nm emission bands) under nitrogen atmosphere increased (**Figure 3a** (i)) as compared to ambient conditions (Figure 3a (ii)). Nevertheless, the bubbling of oxygen gas caused a drop in the PL intensity (Figure 3a (iii)), indicating the involvement of the triplet state in  $[Au_2Cu_6(Sadm)_6(DPPEO)_2]$  NC emission. At the same time, the UV/Vis absorption spectra of

15214095, 2025, 35, Downloaded from https://advanced.onlinelibrary.wiley.com/doi/10.1002/adma.202507893 by Edakkatuparambil Sidharth Shibu - University Of Calicut , Wiley Online Library on [07/09/2025]. See the Terms and Conditions (https://onlinelibrary.wiley.com/term

and-conditions) on Wiley Online Library for rules of use; OA articles are governed by the applicable Creative Commons License

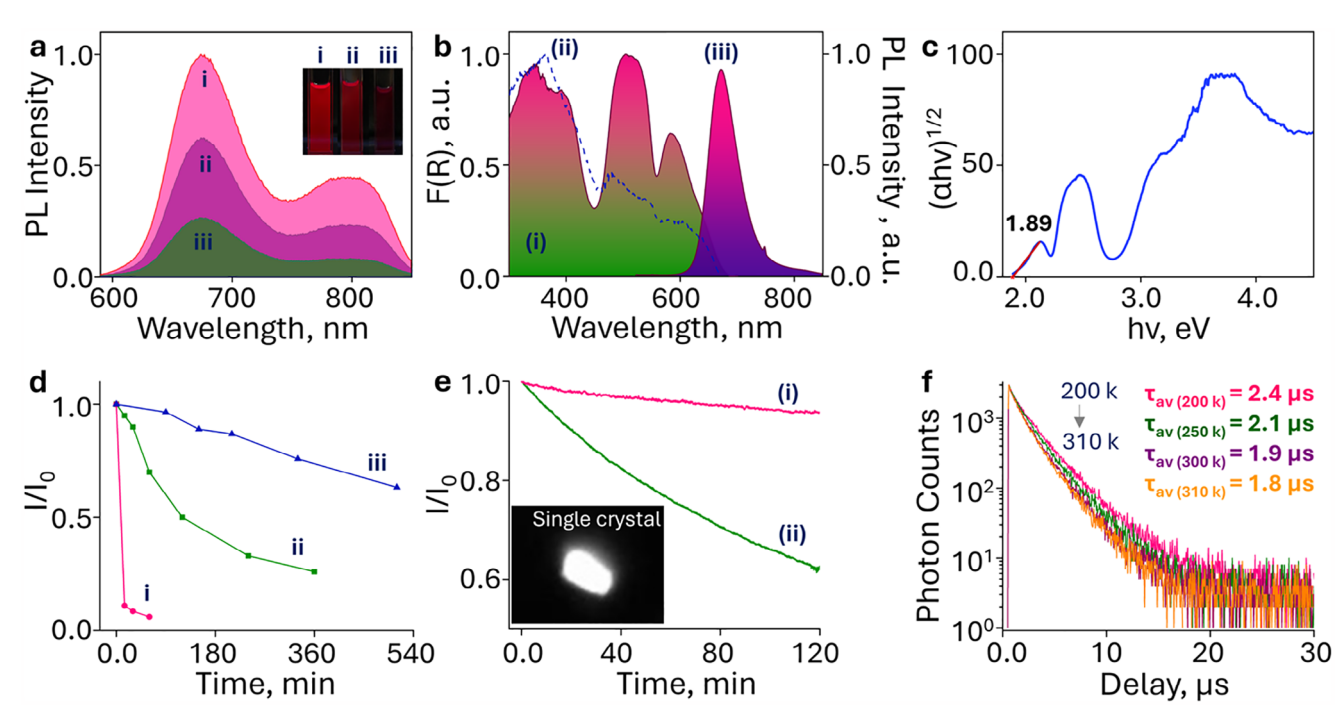


Figure 3. a) PL spectra of NC solution ( $\approx$ 50 μm) recorded under (i) argon, (ii) ambient, and (iii) oxygen atmospheres. The photographs of corresponding solutions are shown in the inset. b) Normalized solid-state absorption (i); converted from DRS using Kubelka-Munk function), excitation (ii) and PL spectra (iii) of [Au<sub>2</sub>Cu<sub>6</sub> (Sadm)<sub>6</sub> (DPPEO)<sub>2</sub>] NC (under 325 nm excitation). c) Tauc plot of [Au<sub>2</sub>Cu<sub>6</sub> (Sadm)<sub>6</sub> (DPPEO)<sub>2</sub>] NC. d) Plots of I/I<sub>0</sub> vs illumination time for (i) NC solution, and (ii and (iii) NC film under (i and ii) ambient, and (iii) inert atmospheres. e) Plots of I/I<sub>0</sub> vs illumination time for a single NC crystal under (i) argon and (ii) oxygen/air atmospheres. The photograph of the single crystal is shown in the inset. f) Temperature-dependent PL decay profiles of [Au<sub>2</sub>Cu<sub>6</sub> (Sadm)<sub>6</sub> (DPPEO)<sub>2</sub>] NC solid under inert atmosphere.

the NC solution (toluene) under argon and oxygen atmospheres showed unaltered optical absorption features (Figure S5, Supporting Information). A similar PL enhancement and quenching was also observed in [Au<sub>2</sub>Cu<sub>6</sub>(Sadm)<sub>6</sub>(TPP)<sub>2</sub>] NC solution, when purged under nitrogen and oxygen gases, respectively (Figure S6, Supporting Information). The solid-state emission of NCs is an important property for their use in real-world devices. The solid-state diffuse reflectance spectrum (DRS) and PL spectrum of [Au<sub>2</sub>Cu<sub>6</sub>(Sadm)<sub>6</sub>(DPPEO)<sub>2</sub>] NC solid (the reflectance spectrum has been converted to absorption spectrum using the Kubelka-Munk function) revealed that the absorbance features observed initially at 425, 515, and 594 nm in solution became broader and slightly blue shifted to 390, 510, and 584 nm, respectively. More importantly, the emission peak at 798 nm diminished drastically, while the 675 nm emission shifted slightly to 672 nm and remained prominent (Figure 3b). A similar trend was observed in the case of [Au<sub>2</sub>Cu<sub>6</sub>(Sadm)<sub>6</sub>(TPP)<sub>2</sub>] NC (Figure \$7, Supporting Information). The dominance of higher-energy emissive states (672 nm) in the solid-state likely arises due to the suppression of longer-wavelength emission, which is attributed to restricted molecular motions or the enhancement of non-radiative decay pathways. These observations suggest that the solid-state environment is crucial in activating a specific radiative channel, favoring a single dominant emission ≈672 nm. The optical bandgap of [Au<sub>2</sub>Cu<sub>6</sub>(Sadm)<sub>6</sub>(DPPEO)<sub>2</sub>] NC solid is calculated from the Tauc plot and found to be 1.89 eV (Figure 3c). Electrochemical differential pulse voltammetry (DPV) was used to investigate the electrochemical band gap of the  $[Au_2Cu_6(Sadm)_6(DPPEO)_2]$ . As shown in Figure S8 (Supporting Information), the LUMO level is located at -3.05 eV with respect to the vacuum level (-1.93 V vs.  $Ag/Ag^+$ ), and the HOMO level is located at  $\approx 5.34$  eV (+0.36 V vs.  $Ag/Ag^+$ ), giving an electronic bandgap of  $\approx 2.29$  eV.

The photostability of NCs in both solution and solid-state (film) was examined by comparing their PL intensity before and after exposure to UV light (365 nm; low power) at different time intervals. A plot of  $I/I_0$  ( $I_0$  represents the PL intensity at t=0) vs. illumination time shows better photostability for NC film under an argon atmosphere (Figure 3d (iii)) compared to the ambient condition (Figure 3d (ii)) or its solution under ambient condition (Figure 3d (i)). Though the NC solution photobleached within 60 min of illumination, the NC film withstood longer, as evident from the UV/Vis spectra recorded under UV light exposure (Figure S9a,b, Supporting Information). The intact optical absorption features of the NC film after UV exposure revealed the photostability of NC in the ensemble solidstate. The photostability of single crystals was also evaluated under different gaseous atmospheres. Before exposure to a highpower CW (continuous-wave) laser (512 nm), the single crystals placed inside a plastic petri dish were sealed and purged with argon gas using a syringe needle. The PL intensity trajectory of a single-crystal under an argon atmosphere showed stable photon counts (Figure 3e (i)). However, the crystals photobleached quickly when the argon was replaced with oxygen or air (Figure 3e (ii)). The photograph of a single crystal used for the experiment is shown in the inset of Figure 3e. The overall data suggest that the

www.advancedsciencenews.com

ADVANCED MATERIALS

vww.advmat.de

15214055, 2025, 35, Dowloaded from https://abranced.online.bitabry.wiely.com/oi/010.1002adma.2025/993 by Edakatunparambil Sidharth Shibu - University Of Calicu, Wiley Online Library on [07/99/2025], See the Terms and Conditions (https://oininelibrary.wiely.com/etms-and-conditions) on Wiley Online Library for rules of use; OA articles are governed by the apaptic between the common in Library on [07/99/2025]. See the Terms and Conditions (https://oininelibrary.wiely.com/etms-and-conditions) on Wiley Online Library for rules of use; OA articles are governed by the apaptic between [07/99/2025]. See the Terms and Conditions (https://oininelibrary.wiely.com/etms-and-conditions) on Wiley Online Library for rules of use; OA articles are governed by the apaptic between [07/99/2025]. See the Terms and Conditions (https://oininelibrary.wiely.com/etms-and-conditions) on Wiley Online Library for rules of use; OA articles are governed by the apaptic between [07/99/2025]. See the Terms and Conditions (https://oininelibrary.wiely.com/etms-and-conditions) on Wiley Online Library for rules of use; OA articles are governed by the apaptic between [07/99/2025]. See the Terms and Conditions (https://oininelibrary.wiely.com/etms-and-conditions) on Wiley Online Library for rules of use; OA articles are governed by the apaptic between [07/99/2025]. See the Terms and Conditions (https://oininelibrary.wiely.com/etms-and-conditions) on the apaptic between [07/99/2025]. See the Terms and Conditions (https://oininelibrary.wiely.com/etms-and-conditions) on the apaptic between [07/99/2025]. See the Terms and Conditions (https://oininelibrary.wiely.com/etms-and-conditions) on the apaptic between [07/99/2025]. See the Terms and Conditions (https://oininelibrary.wiely.com/etms-and-conditions) on the apaptic between [07/99/2025].

photostability of NC is better when the crystals are stored under an inert atmosphere. The thermogravimetric analysis (TGA) revealed that the NC powder remained stable up to 200 °C (Figure \$10, Supporting Information). We further investigated the decay profile of NC in detail. The average lifetime  $(\tau_{av})$  and PLQY of [Au<sub>2</sub>Cu<sub>6</sub>(Sadm)<sub>6</sub>(DPPEO)<sub>2</sub>] NC solid (under vacuum) were found to be 1.9 µs (Figure S11, Supporting Information) and 62%, respectively. The long-excited state lifetime suggests that the triplet excitons are involved in the emission process. This excited state lifetime may be due to phosphorescent emission (triplet  $(T_1)$  to singlet (S<sub>0</sub>)) or thermally activated delayed fluorescence (TADF) emission  $(T_1-S_1-S_0)$ . To further confirm whether it is a phosphorescent emitter or TADF emitter, the temperature-dependent PL spectra (Figure \$12, Supporting Information) and decay profiles (Figure 3f) were measured under vacuum by sandwiching the NC powder between two quartz plates. As shown in Figure S12 (Supporting Information) and Figure 3f, a temperature sweep between 310 to 200 K was carried out. The PL intensity and lifetime values (1.8 to 2.4 µs) were increased when the temperature decreased from 310 to 200 K. The increase in PL intensity and delayed lifetime is due to the decreased molecular vibrations at low temperatures, which decreases the non-radiative channels and results in efficient harvesting of the triplet state at low temperatures. Therefore, the increase in PL intensity with a decrease in temperature and delayed lifetime in microseconds shows that the emission comes mainly from the  $T_1$  to the  $S_0$  state. This confirms that [Au<sub>2</sub>Cu<sub>6</sub>(Sadm)<sub>6</sub>(DPPEO)<sub>2</sub>] NC is a phosphorescent emitter and not the TADF emitter.[59]

Self-assembly approaches have been utilized to fabricate higher-order NC superstructures and alter the PLQY of luminescent NCs. [65,66] The self-assembly allows restricted intermolecular motions, reduces the rotational degree of freedom of the NC surface ligands, and prevents nonradiative relaxations, thereby amplifying the PL.[67] To explore the solid-state emission behavior and the impact of aggregation/assembly on the photophysical properties of NCs, we further examined the solventinduced aggregation of [Au<sub>2</sub>Cu<sub>6</sub>(Sadm)<sub>6</sub>(DPPEO)<sub>2</sub>] NC solution (tetrahydrofuran; THF) in the presence of a poor solvent such as H<sub>2</sub>O. Remarkably, the purple-colored NC solution maintained its optical transparency even as the water volume fraction (f<sub>w</sub> =  $vol_{water}/vol_{THF+water}$ ) increased up to 50%. When the  $f_{w}$  increased from 50% to 90%, the solution turned cloudy with an enhancement in PL intensity (Figure 4a). To understand this phenomenon in detail, we analyzed the changes in PL intensity following the gradual addition of water (Figure 4b). Up to a 40% water fraction, no significant visual or PL changes were observed. However, at 50%  $f_w$ , the solution turned cloudy, accompanied by an increase in PL emission ≈675 nm and a slight reduction in the emission  $\approx$ 800 nm. Notably, at 60%  $f_w$ , the lower-wavelength emission blue-shifted slightly to 672 nm and became dominant, while the higher-wavelength emission ≈800 nm has been completely suppressed. When the water content increased from 70% to 90%, the overall emission intensity was found to decrease compared to 60% f<sub>w</sub>. These trends in PL spectra (Figure 4c) strongly suggest that the restricted molecular movement of ligands during the aggregation/assembly of NCs induces a specific emissive channel, favoring a single, dominant emission.

The TEM (Figure \$13, Supporting Information) and field emission scanning electron microscopy (FESEM; Figure 4d) im-

ages of NC solutions at different f<sub>w</sub> revealed spherical assemblies in all cases. However, the average diameter (size of the spheres) increased from 50% (≈140 nm) to 60% (≈250 nm) and then decreased systematically from 70% (≈150 nm) to 90% (≈70 nm). The results were in agreement with the dynamic light scattering (DLS) data (Figure S14, Supporting Information). Notably, the size of the spherical assemblies was found to be maximum when f<sub>w</sub> is 60%, which is in good agreement with maximum intensity in the PL spectra (Figure 4b) and the scattering in the UV/Vis absorption spectra of NC solution at different f<sub>w</sub> (Figure S15, Supporting Information). The atomic force microscopy (AFM) revealed the average thickness and diameter of a single sphere ≅ 200 and 250 nm, respectively (Figure S16, Supporting Information). The agreement in the size of the spherical assemblies in AFM, TEM, FESEM images, and DLS suggests the presence of spherical assemblies in the solution and not due to the possibility of evaporation-induced assemblies. The scanning transmission electron microscopy (STEM) image and elemental mapping revealed the presence of gold, copper, sulfur, phosphorus, and oxygen (Figure 4e; Figures S17 and S18, Supporting Information). To further understand the 3D internal structure of the assembly, TEM electron tomography (ET) reconstruction was performed (Figure 4f).[68] For 3D reconstruction, 2D TEM projections were collected by tilting the specimen between  $\pm 70^{\circ}$  with an increment angle of 2° (Figure S19, Supporting Information). The aligned tilt series suggests a spherical nature of the superstructure. The 3D reconstruction and cross-sectional views show the presence of densely packed NCs in the assembled spheres (Video S1, Supporting Information). The ET reconstruction data agree with AFM, FESEM, and TEM, as shown above. Importantly, a slight deformation is observed in all spherical particles due to strong adhesion to the carbon support film of the TEM grid. [69] The densely packed structure further suggests that the enhanced PL intensity is presumably due to the restricted rotation of ligands that reduces the non-emissive relaxation pathways.

To investigate the electroluminescence (EL) performance of [Au<sub>2</sub>Cu<sub>6</sub>(Sadm)<sub>6</sub>(DPPEO)<sub>2</sub>] NCs, a non-doped device was fabricated with the following device architecture: Glass/ITO/PEDOT: PSS (40 nm)/PVK (30 nm)/[Au<sub>2</sub>Cu<sub>6</sub>(Sadm)<sub>6</sub>(DPPEO)<sub>2</sub>] NCs (25 nm)/TPBi (50 nm)/Liq (2 nm)/Al (100 nm) (Figure 5a). The chemical structures of different layers used in the device fabrication is shown in Figure S20 (Supporting Information). The device performance characteristics are shown in Figure 5b-f and summarized in Table 1 and Video S2 (Supporting Information). The EQE vs. luminance curve shows an EQE<sub>max</sub> of 12.60% with a turn-on voltage of 3V. The J-V-L (current density vs voltage vs luminance) curve shows a maximum current density of 387 mA cm<sup>-2</sup> and a maximum luminance of 1246 cd m<sup>-2</sup>. The device shows the maximum current efficiency (CE<sub>max</sub>) and power efficiency (PE<sub>max</sub>) of 3.7 cd A<sup>-1</sup> and 3.8 lm  $\ensuremath{W^{-1}}$ , respectively. The EL spectra show a maximum EL wavelength ( $\lambda_{EI}$ ) of 668 nm with the CIE coordinates of (0.70 and 0.30), and FWHM (full-width half maximum) of 72 nm. The CIE coordinates of the [Au<sub>2</sub>Cu<sub>6</sub>(Sadm)<sub>6</sub>(DPPEO)<sub>2</sub>] NCs-based device are located at the edge of the chromaticity diagram, which represents the most saturated red color light. The EL spectra of [Au<sub>2</sub>Cu<sub>6</sub>(Sadm)<sub>6</sub>(DPPEO)<sub>2</sub>] NCs-based device were also taken at various voltages (5-10 V; Figure 5b), and no significant residual emission peak was observed. This indicates that the

from https://advanced.onlinelibrary.wiley.com/doi/10.1002/adma.202507893 by Edakkattuparambil Sidharth Shibu - University Of Calicut , Wiley Online Library on [07/09/2025]. See the Terms and Conditions (https://advanced.onlinelibrary.wiley.com/doi/10.1002/adma.202507893 by Edakkattuparambil Sidharth Shibu - University Of Calicut , Wiley Online Library on [07/09/2025]. See the Terms and Conditions (https://advanced.onlinelibrary.wiley.com/doi/10.1002/adma.202507893 by Edakkattuparambil Sidharth Shibu - University Of Calicut , Wiley Online Library on [07/09/2025]. See the Terms and Conditions (https://advanced.onlinelibrary.wiley.com/doi/10.1002/adma.202507893 by Edakkattuparambil Sidharth Shibu - University Of Calicut , Wiley Online Library on [07/09/2025]. See the Terms and Conditions (https://advanced.onlinelibrary.wiley.com/doi/10.1002/adma.202507893 by Edakkattuparambil Sidharth Shibu - University Of Calicut , Wiley Online Library on [07/09/2025].

conditions) on Wiley Online Library for rules of use; OA articles are governed by the applicable Creative Commons License

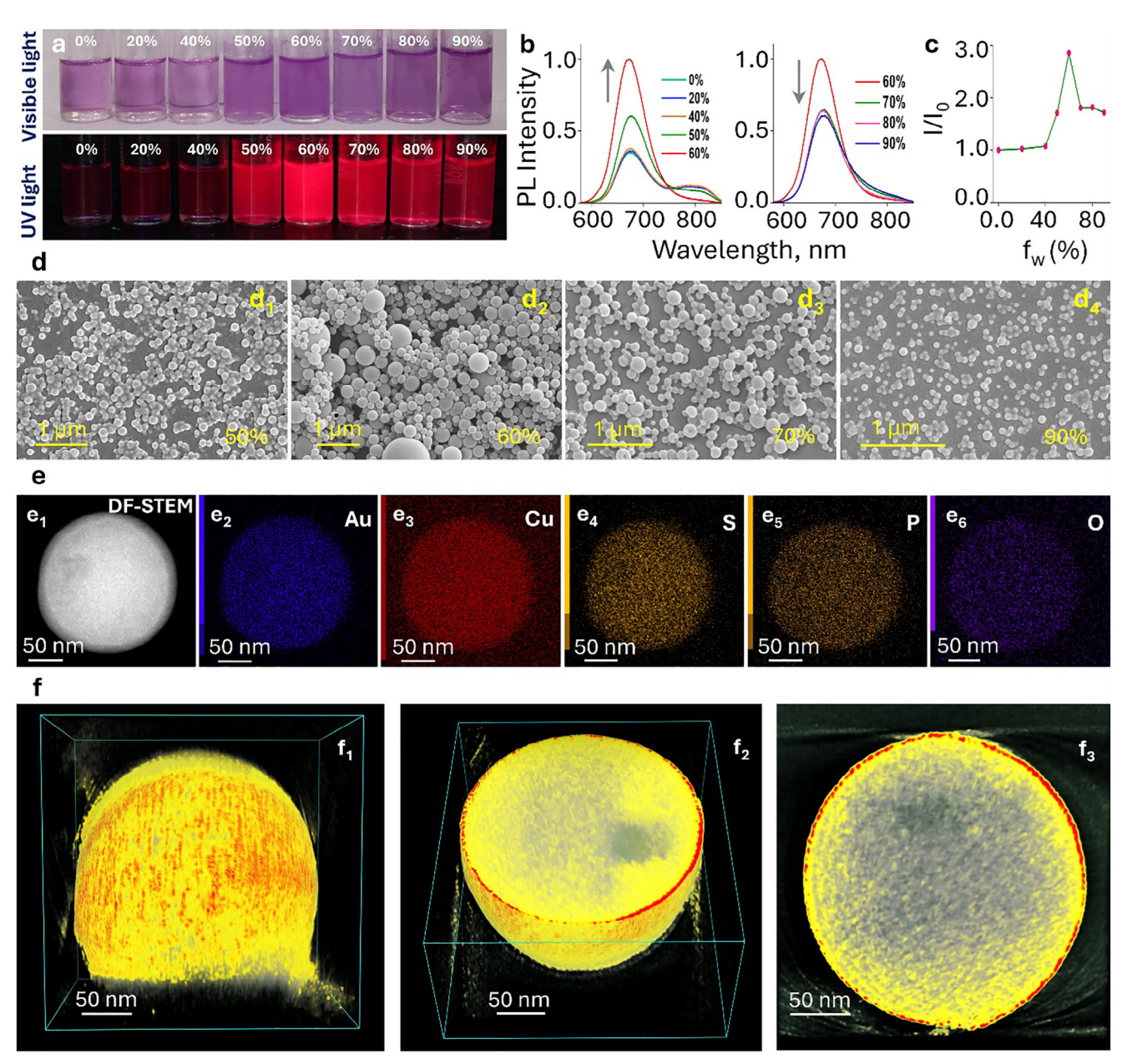


**Figure 4.** a) Photographs of NC solution (under visible and UV light) prepared in different  $f_w$ . The corresponding PL spectra are shown in Figure 4b. A Plot of  $I/I_0$  vs  $f_w$  is shown in Figure 4c. d) FESEM images of NC assembly fabricated at  $(d_1)$  50%,  $(d_2)$  60%,  $(d_3)$  70%, and  $(d_4)$  90%  $f_w$ .  $(e_1)$  STEM image  $(60\% f_w)$  and elemental maps of a single sphere showing  $(e_2)$  gold,  $(e_3)$  copper,  $(e_4)$  sulfur,  $(e_5)$  phosphorus, and  $(e_6)$  oxygen.  $(f_1)$  3D reconstructed structure of the superstructures showing spherical assembly, and  $(f_2)$  and  $(f_3)$  shows the cross-sectional view suggesting densely packed NCs.

fabricated [Au<sub>2</sub>Cu<sub>6</sub>(Sadm)<sub>6</sub>(DPPEO)<sub>2</sub>] NCs-based device is very stable under different operating voltages, and the electron–hole recombination occurs within the emissive layer at different operating voltages. To evaluate the device's performance, the energy level alignment of the device was also analyzed (Figure S21, Supporting Information). The NC has a HOMO at  $\approx$ 5.34 eV and LUMO at  $\approx$ 3.05 eV (from DPV measurements), which suggests a reduced hole injection barrier (from PVK) and a moderate electron injection barrier (from TPBi). This energy alignment supports balanced carrier injection, reduced charge leakage, and efficient exciton confinement within the emis-

sive layer. Compared to the previous reports, the exceptional device performance demonstrates that this is one of the first solution-processed non-doped NC-based devices holding high EQE and a deeply saturated red emission. As a control, we also fabricated the device with  $[\mathrm{Au_2Cu_6(Sadm)_6(TPP)_2}]$  NCs as an emissive layer in a similar device structure (Figure S22, Supporting Information). The EQE of  $[\mathrm{Au_2Cu_6(Sadm)_6(TPP)_2}]$  NC-based device was found to be only 3.24%, which is much less compared to  $[\mathrm{Au_2Cu_6(Sadm)_6(DPPEO)_2}]$  NC-based device (details are provided in Table 1). The performance comparison of  $[\mathrm{Au_2Cu_6(Sadm)_6(DPPEO)_2}]$  NC with previous reports is provided

15214095, 2025, 35, Downloaded from https://advanced.onlinelibrary.wiley

.com/doi/10.1002/adma.202507893 by Edakkatuparambil Sidharth Shibu - University Of Calicut , Wiley Online Library on [07/09/2025]. See the Terms and Conditions (https://onlinelibrary.wiley.com/tern

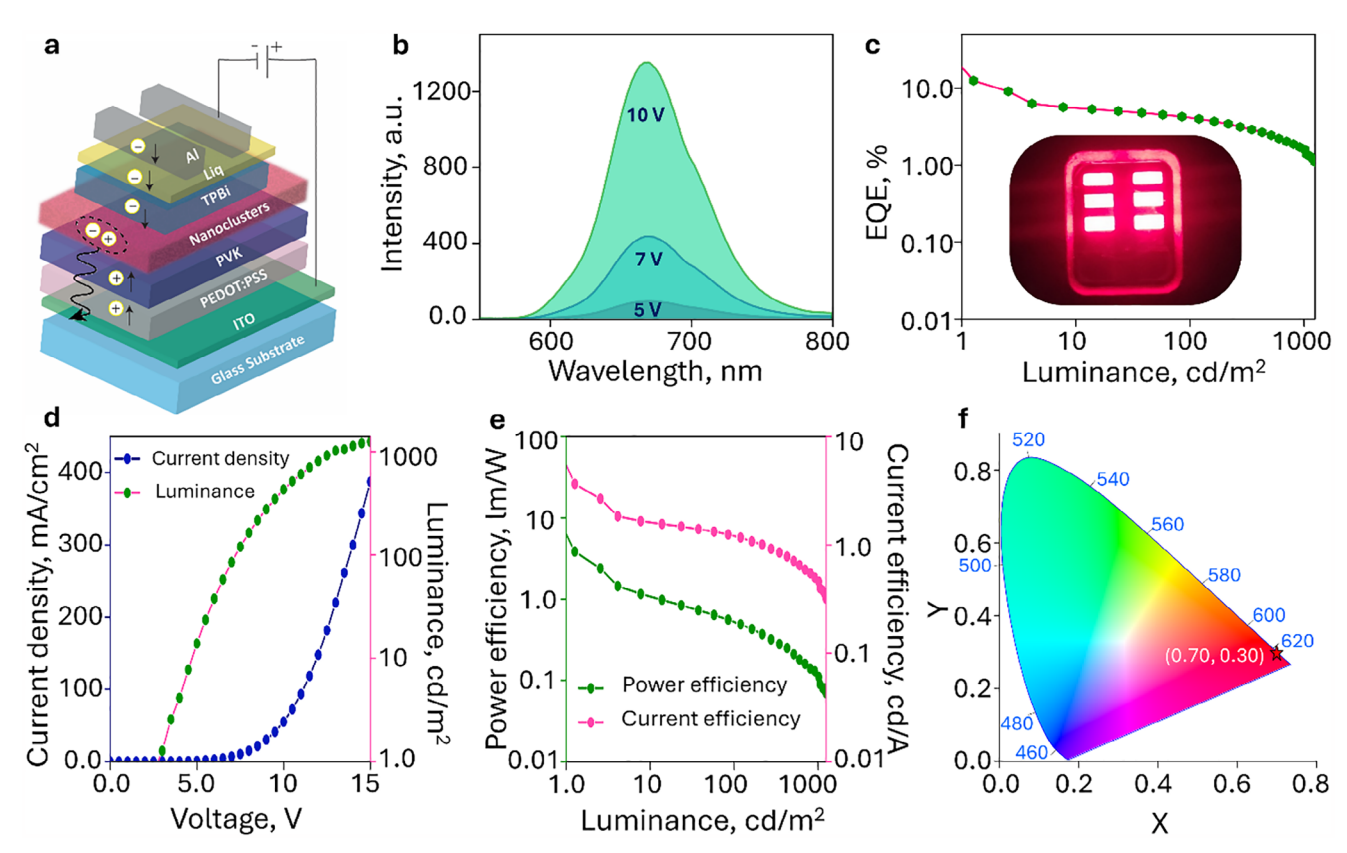


Figure 5. a) A schematic of the LED device. b) EL spectra of the device at 5, 7, and 10V. c) EQE vs luminance curve. The inset shows a photograph of the fabricated LED device. d) Current density-voltage-luminance (*J*–*V*–*L*) curves of the device. e) Power efficiency-luminance-current efficiency curves of the device. f) Chromaticity diagram of the device.

in the Table S1 (Supporting Information). The table shows that  $[Au_2Cu_6(Sadm)_6(DPPEO)_2]$  NC performs the best in a solution-processed non-doped device with saturated red emission. This study not only demonstrates the high performance of the device but also looks into how ligand design can improve PLQY and overall performance. These NCs are expected to play an important role in developing next-generation LEDs.

#### 3. Conclusion

In summary, we have successfully demonstrated the fabrication of NC-LED using the solid-state emitting  $[Au_2Cu_6(Sadm)_6(DPPEO)_2]$  NCs. The gold-copper bimetallic NCs synthesized using the magical combination of HSadm and DPPE ligands showed rapid crystallization during

solvent evaporation. These NCs showed exceptional photostability when their crystals/films were preserved under inert conditions. The NCs displayed solvent-induced aggregation behavior, resulting in spherical superstructures and self-assembly with enhanced PL. Multiple spectroscopic and microscopic techniques have been employed to study the assembly and morphology of superstructures. The average diameter of assembled superstructures was found to be at a maximum of 60% volume fraction, which was systematically reduced by increasing the volume fraction. DLS data were in good agreement with TEM and FESEM micrographs. HRTEM, ET reconstruction, AFM, and FESEM data revealed the presence of thickly packed NCs in the assembled superstructures. The restricted molecular movement of ligands during the aggregation/assembly of NCs helped to reduce the

**Table 1.** The summary of device characteristics.

Emitting layer	Turn-on Voltage [V] @ 1 cd m <sup>-2</sup>	Current density [J <sub>max</sub> ] mA cm <sup>-2</sup>	L <sub>max</sub> [cd m <sup>-2</sup> ]	EQE <sub>max</sub> [%]	CE <sub>max</sub> [cd A <sup>-1</sup> ]	PE <sub>max</sub> [lm W <sup>-1</sup> ]	λ[EL] <sub>max</sub> [nm]	CIE [x, y]	FWHM [nm]
	3.0	387.42 (@ 15	1246 (@ 15 V)	12.60	3.70	3.80	668	(0.70, 0.30)	72.00
$[Au_2Cu_6(Sadm)_6(DPPEO)_2]$		V)							
$[Au_2Cu_6(Sadm)_6(TPP)_2]$	5.8	54.55 (@ 15 V)	55.17 (@ 15 V)	3.24	2.31	1.21	666	(0.67, 0.31)	68.47

 $L_{max} = maximum$  luminance, EQE<sub>max</sub> = maximum external quantum efficiency, CE<sub>max</sub> = maximum current efficiency, PE<sub>max</sub> = maximum power efficiency,  $\lambda$ (EL)<sub>max</sub> = electroluminescent maximum wavelength.

15214095, 2025, 35, Downloaded from https://advanced.onlinelibrary.wiley.com/doi/10.1002/adma.202507893 by Edakkattparambil Sidharth Shibu - University Of Calicut, Wiley Online Library on [07/09/2025]. See the Terms and Conditions (https://onlinelibrary.wiley.com/terms-

and-conditions) on Wiley Online Library for rules of use; OA articles are governed by the applicable Creative Commons License

non-emissive relaxation pathways. Finally, the NC-LED has been fabricated using the solution-processed technique without using any additional host materials. The fabricated NC-LED showed a maximum brightness of 1246 cd m<sup>-2</sup> and an EQE of 12.60% with a saturated pure red emission. This EQE value with saturated deep red emission is the best among solution-processed, non-doped NC-LED devices. The results presented in the work suggest the potential of NCs for the fabrication of sustainable, non-toxic, and efficient LEDs in the future.

### 4. Experimental Section

Reagents and Materials: All the chemicals and solvents are analytical grade and used without any further purification.  $Chloro(dimethylsulfide) gold (I) \qquad ((CH_3)_2 SAuCl), \quad copper \quad (II) \quad nitrate$ trihydrate (Cu(NO<sub>3</sub>)<sub>2</sub>·3H<sub>2</sub>O), 1-adamantanethiol (HSadm), and sodium borohydride (NaBH<sub>4</sub>) were purchased from Sigma-Aldrich. 1,2-bis(diphenylphosphino)ethane (DPPE) and triphenylphosphine (TPP) were purchased from Tokyo Chemical Industry (TCI) Co. Ltd. Japan. Acetonitrile (ACN), dichloromethane (DCM), tetrahydrofuran (THF), toluene, ethanol, hexane, and chloroform-d (CDCl<sub>3</sub>) were purchased from Sisco Research Laboratories (SRL). The different chemical layers used for the device fabrication were purchased commercially. Poly(3,4-ethylenedioxythiophene) polystyrene sulfonate (PEDOT: PSS) was purchased from Ossila Ltd. Polyvinyl carbazole (PVK) was purchased 2,2',2"-(1,3,5-benzinetriyl)-tris(1-phenyl-1-H-Sigma-Aldrich. benzimidazole) (TPBi) and lithium-8-hydroxyquinolinolate (Liq) were purchased from BLD Pharmatech (India) Pvt. Ltd. PEDOT: PSS and PVK were used as received, whereas TPBi and Liq were further purified by vacuum sublimation before the device fabrication.

Instrumentation: The <sup>1</sup>H and <sup>31</sup>P NMR measurements were carried out using Bruker, AVANCE III HD 400/500 MHz spectrometers. UV/Vis absorbance and DRS spectra were recorded in the JASCO-V-750 spectrophotometer. PL spectra were recorded using a PerkinElmer LS55 Spectrofluorimeter. Optical images of crystallized NCs were recorded using a Leica optical microscope. Absolute PLQY measurements and temperaturedependent PL lifetime of NC powder were carried out using an Edinburgh FLS 100 Fluorescence lifetime spectrometer (510 nm diode laser). The fluorescent image of the NC crystal was captured using an Olympus CKX53 inverted microscope (435 nm excitation). DLS measurements were performed in Zetasizer Nano S90 (Malvern). ESI-MS measurements were carried out on a Waters Synapt G2-Si high-definition mass spectrometer. DPV was performed using an Electrochem SAS OrigaLys electrochemical workstation at room-temperature. Measurements were carried out in a deaerated ACN/toluene mixture with tetrabutylammonium hexafluorophosphate as the supporting electrolyte. A glassy carbon electrode was used as the working electrode, with a Pt wire as the counter electrode and Ag/Ag<sup>+</sup> as the reference electrode. Ferrocene/ferrocenium (Fc/Fc<sup>+</sup>) served as the internal standard, and all potential energy levels of a molecular orbital (MO) relative to vacuum level by  $E_{MO}$  (V, vs. NHE) =  $-E_{MO}$ (eV, vs. Vacuum level) — 4.44. [57] HR-TEM images were recorded on a FEI Talos F200S (200 kV) TEM and JEOL 3010 (300 kV) TEM. A Jeol F200 STEM electron microscope operated at 200 keV was used for STEM images with EDS and elemental mapping and collecting data for 3D electron tomographic reconstruction. For tomographic reconstruction, 2D projections were collected between  $\pm$  70° with increment angles of 2°. The acquired raw 2D projections were first subjected to a series of pre-processing using the IMOD software package.<sup>[70,71]</sup> Coarse alignment was used to create the aligned file. The custom-made maximum entropy method (MEM) program was used for 3D reconstruction. [72,73] Chimera was used to produce colored images. FESEM analysis was performed with a Verios G4 UC, FEI instrument. The samples were sputter-coated with an Au/Pd mixture to produce better-quality images without charging. AFM images were captured using an Agilent Technologies 5500 series AFM/SPM microscope equipped with Pico View 1.14.1 software, and finally, images were processed using Gwyddion. XPS spectra were recorded using a Thermo Scientific ESCALAB 250Xi (XR6 Micro-focused Monochromator, Al K $\alpha$ ). SCXRD data collection was performed using a Bruker D8 VENTURE single-crystal X-ray diffractometer. TGA was carried out using a TA Instrument Model SDT Q600. Silicon photodiode with Keithley 2450 source meter and Keithley 2100 multimeter were used to measure the current-voltage-luminescence (J-V-L) characteristics. The EL spectra were obtained using a Hitachi F-7100 fluorescence spectrophotometer.

Synthesis of  $[Au_2Cu_6(Sadm)_6(TPP)_2]$  NCs:  $[Au_2Cu_6(Sadm)_6(TPP)_2]$  NCs were synthesized using the previously reported protocol. [59]

Synthesis of  $[Au_2Cu_6(Sadm)_6(DPPEO)_2]$  NCs: Briefly,  $(CH_3)_2SauCl(30 mg; 0.1 mmol)$  and DPPE (80 mg; 0.2 mmol) were dissolved in 10 mL DCM. In parallel,  $Cu(II)NO_3 \cdot 3H_2O$  (50 mg; 0.2 mmol) was dissolved in 5 mL  $CH_3CN$  using ultrasonication. The addition of the freshly prepared copper salt solution into the stirring ( $\approx 1000 \text{ rpm}$ ) solution of gold/DPPE mixture prepared in DCM produced a greenish solution within 15 min of the reaction. The addition of HSadm (68 mg; 0.4 mmol) into the above-prepared greenish solution turned it colorless. To this colorless solution kept at 0 °C,  $NaBH_4$  (40 mg (1 mmol) in 5 mL ethanol) was injected and stirred vigorously for another 20 h till a purple-colored precipitate was formed. The precipitate was washed independently with  $CH_3CN$  and hexane, extracted in DCM, and the final rotary evaporation produced a purple-colored NC powder. All the reactions were performed under dark conditions in an ambient atmosphere. The yield of the NC is 85% with respect to Cu.

## **Supporting Information**

Supporting Information is available from the Wiley Online Library or from the author.

## Acknowledgements

E.S.S. thanks SERB (Science and Engineering Research Board) and DST (Department of Science and Technology), India for the Ramanujan Fellowship (SB/S2/RJN-005/2017), Startup Research grant (SRG/2022/586), and Promotion of University Research and Scientific Excellence grant (SR/PURSE/2023/191). E.S.S. thanks Kerala State Council for Science - Environment (KSCSTE) for the SRS grant (123/2025/KSCSTE) and the University of Calicut for the seed money grant. E.S.S. and V.B. thank the Japan Society for the Promotion of Science (JSPS) and Hokkaido University for the JSPS-BRIDGE Fellowship program (BR230604). We thank Prof. Subi Jacob George, Miss Anju Ajayan, Dr. Saraswathi Chirakkara, and Miss Gayathri Govind V. (JNCASR, Bangalore) for temperature-dependent lifetime measurements. V. B. acknowledges a MEXT-JSPS Grant-in-Aid for Scientific Research (Kaken-hi 23H01781) and the Hokkaido University Photoexcitonix Program. We thank Dr. Reji Thomas (Farook College, Calicut) for the fluorescence imaging. J.V.R. thanks SERB and the University of Calicut for research fellowships. S.C. thanks the Ministry of Education (MoE), India, for the PMRF fellowship. The authors acknowledge the Research Council of Finland for project funding (352900), the Photonics Research and Innovation (PREIN) flagship, and the Tampere Microscopy Centre for imaging facilities. P.R. thanks the Indian Institute of Science (IISc) and SERB (SPG/2020/000107) for financial support.

#### Conflict of Interest

The authors declare no conflict of interest.

### **Data Availability Statement**

The data that support the findings of this study are available from the corresponding author upon reasonable request.

www.advancedsciencenews.com

# ADVANCED MATERIALS

www.advmat.de

15214095, 2025, 35, Downloaded from https://advanced.onlinelibrary.wiey.com/doi/10.1002/adma.202507993 by Edakkattuparambil Sidharth Shibu - University Of Calicut, Wiley Online Library on [07/09/2025]. See the Terms and Conditions (https://onlinelibrary.wiley.com/ter

and-conditions) on Wiley Online Library for rules of use; OA articles are governed by the applicable Creative Commons

#### Keywords

bimetallic nanocluster, light-emitting diodes, supramolecular assembly, phosphorescence, electroluminescence

Received: April 25, 2025 Published online: June 11, 2025

- [1] Y. Shirasaki, G. J. Supran, M. G. Bawendi, V. Bulović, *Nat. Photonics* **2013**, *7*, 13.
- [2] J. H. Burroughes, D. D. C. Bradley, A. R. Brown, R. N. Marks, K. Mackay, R. H. Friend, P. L. Burns, A. B. Holmes, *Nature* 1990, 347, 539.
- [3] A. Zampetti, A. Minotto, F. Cacialli, Adv. Funct. Mater. 2019, 29, 1807623.
- [4] B. Van der Zee, Y. Li, G.-J. A. H. Wetzelaer, P. W. M. Blom, Adv. Mater. 2022, 34, 2108887.
- [5] L. Protesescu, S. Yakunin, M. I. Bodnarchuk, F. Krieg, R. Caputo, C. H. Hendon, R. X. Yang, A. Walsh, M. V. Kovalenko, *Nano Lett.* 2015, 15, 3692.
- [6] S.-J. Zou, Y. Shen, F.-M. Xie, J.-D. Chen, Y.-Q. Li, J.-X. Tang, Mater. Chem. Front. 2020, 4, 788.
- [7] E. Jang, H. Jang, Chem. Rev. 2023, 123, 4663.
- [8] N. Wang, L. Cheng, R. Ge, S. Zhang, Y. Miao, W. Zou, C. Yi, Y. Sun, Y. Cao, R. Yang, Y. Wei, Q. Guo, Y. Ke, M. Yu, Y. Jin, Y. Liu, Q. Ding, D. Di, L. Yang, G. Xing, H. Tian, C. Jin, F. Gao, R. H. Friend, J. Wang, W. Huang, Nat. Photonics 2016, 10, 699.
- [9] L. G. Franca, D. G. Bossanyi, J. Clark, P. L. Dos Santos, ACS Appl. Opt. Mater. 2024, 2, 2476.
- [10] Z. Yang, M. Gao, W. Wu, X. Yang, X. W. Sun, J. Zhang, H.-C. Wang, R.-S. Liu, C.-Y. Han, H. Yang, W. Li, Mater. Today 2019, 24, 69.
- [11] X. Zhao, J. D. A. Ng, R. H. Friend, Z.-K. Tan, ACS Photonics 2018, 5, 3866.
- [12] H. Qian, M. Zhu, Z. Wu, R. Jin, Acc. Chem. Res. 2012, 45, 1470.
- [13] I. Chakraborty, T. Pradeep, Chem. Rev. 2017, 117, 8208.
- [14] R. Jin, C. Zeng, M. Zhou, Y. Chen, Chem. Rev. 2016, 116, 10346.
- [15] K. Kwak, V. D. Thanthirige, K. Pyo, D. Lee, G. Ramakrishna, J. Phys. Chem. Lett. 2017, 8, 4898.
- [16] L. G. AbdulHalim, M. S. Bootharaju, Q. Tang, S. Del Gobbo, R. G. AbdulHalim, M. Eddaoudi, D. Jiang, O. M. Bakr, J. Am. Chem. Soc. 2015, 137, 11970.
- [17] J. V. Rival, P. Mymoona, R. Vinoth, A. M. V. Mohan, E. S. Shibu, ACS Appl. Mater. Interfaces 2021, 13, 10583.
- [18] M. Xie, C. Han, Q. Liang, J. Zhang, G. Xie, H. Xu, Sci. Adv. 2019, 5, aav9857.
- [19] N. Zhang, Y. Li, S. Han, Y. Wei, H. Hu, R. Huo, C. Duan, J. Zhang, C. Han, G. Xie, H. Xu, Angew. Chem., Int. Ed. 2023, 62, 202305018.
- [20] H. Häkkinen, Chem. Soc. Rev. 2008, 37, 1847.
- [21] T. Chen, S. Yang, J. Chai, Y. Song, J. Fan, B. Rao, H. Sheng, H. Yu, M. Zhu, Sci. Adv. 2017, 3, 1700956.
- [22] Y. Negishi, K. Nobusada, T. Tsukuda, J. Am. Chem. Soc. 2005, 127, 5261.
- [23] S. Knoppe, T. Bürgi, Acc. Chem. Res. 2014, 47, 1318.
- [24] B. Niesen, B. P. Rand, Adv. Mater. 2014, 26, 1446.
- [25] T.-W. Koh, A. M. Hiszpanski, M. Sezen, A. Naim, T. Galfsky, A. Trivedi, Y.-L. Loo, V. Menon, B. P. Rand, *Nanoscale* 2015, 7, 9140.
- [26] L. Xu, J. Wang, X. Zhu, X. Zeng, Z. Chen, Adv. Funct. Mater. 2015, 25, 3033.
- [27] L.-J. Xu, X. Zhang, J.-Y. Wang, Z.-N. Chen, J. Mater. Chem. C 2016, 4, 1787.
- [28] N. Natarajan, L.-X. Shi, H. Xiao, J.-Y. Wang, L.-Y. Zhang, X. Zhang, Z.-N. Chen, J. Mater. Chem. C 2018, 6, 8966.

- [29] N. Natarajan, L.-X. Shi, H. Xiao, J.-Y. Wang, L.-Y. Zhang, X. Zhang, Z.-N. Chen, J. Mater. Chem. C 2019, 7, 2604.
- [30] Y.-Z. Huang, L.-X. Shi, J.-Y. Wang, H.-F. Su, Z.-N. Chen, ACS Appl. Mater. Interfaces 2020, 12, 57264.
- [31] Z. Jiao, M. Yang, J.-Y. Wang, Y.-Z. Huang, P. Xie, Z.-N. Chen, J. Mater. Chem. C 2021, 9, 5528.
- [32] T. Li, Z. Wang, Y. Zhang, Z. Wu, Nanomaterials 2022, 12, 3837.
- [33] X. Zhang, H. Xu, Angew. Chem., Int. Ed. 2023, 136, 202317597.
- [34] J. Lu, B. Shao, R.-W. Huang, L. Gutiérrez-Arzaluz, S. Chen, Z. Han, J. Yin, H. Zhu, S. Dayneko, M. N. Hedhili, X. Song, P. Yuan, C. Dong, R. Zhou, M. I. Saidaminov, S.-Q. Zang, O. F. Mohammed, O. M. Bakr, J. Am. Chem. Soc. 2024, 146, 4144.
- [35] Y. Tian, W. Zheng, X. Zhang, Y. Wang, Y. Xiao, D. Yao, H. Zhang, *Nano Lett.* 2023, 23, 4423.
- [36] X. Kang, Y. Li, M. Zhu, R. Jin, Chem. Soc. Rev. 2020, 49, 6443.
- [37] X. Kang, M. Zhu, Chem. Soc. Rev. 2019, 48, 2422.
- [38] J. V. Rival, P. Mymoona, K. M. Lakshmi, Nonappa, T. P, E. S. Shibu, Small 2021, 17, 2005718.
- [39] M. Jash, A. Jana, A. K. Poonia, E. Khatun, P. Chakraborty, A. Nagar, T. Ahuja, K. V. Adarsh, T. Pradeep, Chem. Mater. 2023, 35, 313.
- [40] S. Chakraborty, D. Bain, S. Maity, S. Kolay, A. Patra, J. Phys. Chem. C 2022, 126, 2896.
- [41] J. V. Rival, Nonappa, E. S. S, ACS Appl. Mater. Interfaces 2020, 12, 14569.
- [42] K. M. Lakshmi, J. V. Rival, P. Sreeraj, S. R. Nambiar, C. Jeyabharathi, Nonappa, E. S. S, Small 2023, 19, 2207119.
- [43] Z. Xie, P. Sun, Z. Wang, H. Li, L. Yu, D. Sun, M. Chen, Y. Bi, X. Xin, J. Hao, Angew. Chem., Int. Ed. 2020, 59, 9922.
- [44] A. K. Das, S. Biswas, S. S. Manna, B. Pathak, S. Mandal, Chem. Sci. 2022, 13, 8355.
- [45] Y. Song, Y. Li, M. Zhou, X. Liu, H. Li, H. Wang, Y. Shen, M. Zhu, R. Jin, Sci. Adv. 2021, 7, abd2091.
- [46] S.-S. Zhang, S. Havenridge, C. Zhang, Z. Wang, L. Feng, Z.-Y. Gao, C. M. Aikens, C.-H. Tung, D. Sun, J. Am. Chem. Soc. 2022, 144, 18305
- [47] A. Jana, M. Jash, W. A. Dar, J. Roy, P. Chakraborty, G. Paramasivam, S. Lebedkin, K. Kirakci, S. Manna, S. Antharjanam, J. Machacek, M. Kucerakova, S. Ghosh, K. Lang, M. M. Kappes, T. Base, T. Pradeep, Chem. Sci. 2023, 14, 1613.
- [48] A. Jana, S. Duary, A. Das, A. R. Kini, S. Acharya, J. Machacek, B. Pathak, T. Base, T. Pradeep, Chem. Sci. 2024, 15, 13741.
- [49] Z. Luo, X. Yuan, Y. Yu, Q. Zhang, D. T. Leong, J. Y. Lee, J. Xie, J. Am. Chem. Soc. 2012, 134, 16662.
- [50] J. Xie, Y. Zheng, J. Y. Ying, J. Am. Chem. Soc. 2009, 131, 888.
- [51] Y. Wang, Z. Liu, A. Mazumder, C. G. Gianopoulos, K. Kirschbaum, L. A. Peteanu, R. Jin, J. Am. Chem. Soc. 2023, 145, 26328.
- [52] S. Takano, H. Hirai, T. Nakashima, T. Iwasa, T. Taketsugu, T. Tsukuda, J. Am. Chem. Soc. 2021, 143, 10560.
- [53] M. Mitsui, D. Arima, Y. Kobayashi, E. Lee, Y. Niihori, Adv. Opt. Mater. 2022, 10, 2200864.
- [54] X.-H. Ma, Y. Si, J.-H. Hu, X.-Y. Dong, G. Xie, F. Pan, Y.-L. Wei, S.-Q. Zang, Y. Zhao, J. Am. Chem. Soc. 2023, 145, 25874.
- [55] Z. Liu, L. Luo, R. Jin, Adv. Mater. 2024, 36, 2309073.
- [56] H. Lin, X. Song, O. J. H. Chai, Q. Yao, H. Yang, J. Xie, Adv. Mater. 2024, 36, 2401002.
- [57] D. Arima, S. Hidaka, S. Yokomori, Y. Niihori, Y. Negishi, R. Oyaizu, T. Yoshinami, K. Kobayashi, M. Mitsui, J. Am. Chem. Soc. 2024, 146, 16630.
- [58] X. Kang, S. Wang, Y. Song, S. Jin, G. Sun, H. Yu, M. Zhu, Angew. Chem., Int. Ed. 2016, 55, 3611.
- [59] D. Arima, Y. Niihori, M. Mitsui, J. Mater. Chem. C 2022, 10, 4597.
- [60] Y. Wei, W. Kan, J. Zhang, H. Xu, Appl. Phys. Lett. 2020, 117, 071901.



#### www.advancedsciencenews.com

ADVANCED MATERIALS

www.advmat.de

15214095, 2025, 35, Downloaded from https://advanced.onlinelibrary.wiley.com/doi/10.1002/adma.202507893 by Edakkattuparambil Sidharth Shibu - University Of Calicut

, Wiley Online Library on [07/09/2025]. See the Terms

and-conditions) on Wiley Online Library for rules of use; OA articles are governed by the applicable Creative Commons License

- [61] C.-H. Lee, M.-C. Tang, W.-L. Cheung, S.-L. Lai, M.-Y. Chan, V. W.-W. Yam, Chem. Sci. 2018, 9, 6228.
- [62] G. Mallesham, C. Swetha, S. Niveditha, M. E. Mohanty, N. J. Babu, A. Kumar, K. Bhanuprakash, V. J. Rao, J. Mater. Chem. C 2015, 3, 1208.
- [63] X. Kang, X. Li, H. Yu, Y. Lv, G. Sun, Y. Li, S. Wang, M. Zhu, RSC Adv. 2017, 7, 28606.
- [64] D. Zhang, P. Pan, X. Du, X. Kang, M. Zhu, Nanoscale 2024, 16, 11513.
- [65] Nonappa, Beilstein J. Nanotechnol. 2020, 11, 533.
- [66] N. Goswami, F. Lin, Y. Liu, D. T. Leong, J. Xie, Chem. Mater. 2016, 28, 4009
- [67] S. Chandra, Nonappa, G. B, A. Som, S. Zhou, J. Lahtinen, H. Jiang, J. V. I. Timonen, O. Ikkala, R. H. A. Ras, Adv. Optical Mater. 2019, 7, 1900620.
- [68] Nonappa, ACS Mater. 2024, 4, 238.
- [69] Nonappa, P. Engelhardt, Imaging Microsc. 2019, 21, 22.
- [70] D. N. Mastronarde, Microsc. Microanal. Microstruct. 2003, 9, 1182.
- [71] D. N. Mastronarde, J. Struct. Biol. 2005, 152, 36.
- [72] P. Engelhardt, in *Electron Microscopy* (Ed: J. Kuo), Humana Press, Totowa, NJ, 2007, pp. 365–385.
- [73] P. Engelhardt, in *Encyclopedia of Analytical Chemistry* (Ed: R.A. Meyers), John Wiley & Sons, Ltd, Chichester, UK, **2006**, p. a1405.